Unimolecular Dissociation Reactions of Methyl Benzoate Radical Cation

Yiqun Huang, Scott Peterman, Shane E. Tichy, Simon W. North, and David H. Russell*

Department of Chemistry, The Laboratory for Biological Mass Spectrometry, Texas A&M University, College Station, Texas 77842

Received: November 12, 2007; Revised Manuscript Received: September 25, 2008

The blackbody infrared radiation induced dissociation of methyl benzoate ($C_8H_8O_2^{+\bullet}$) radical cation was investigated by using a Fourier transfer ion cyclotron resonance mass spectrometer equipped with a resistively heated (wire temperatures of 400−1070 K) wire ion guide. We observed product ion branching ratios that are strongly dependent upon wire temperature. At low temperatures (670−890 K) the major product ion $C_7H_8^{+\bullet}$ (*m*/*z* 92), which is formed by loss of CO_2, and at higher temperatures (above 900 K), loss of methoxy radical ($^{\bullet}OCH_3$) competes with loss of CO_2. The energies of the various reactant ions and transition states for product ion formation were estimated by using density functional theory molecular orbital calculations, and a proposed mechanism for the dissociation chemistry of $C_8H_8O_2^{+\bullet}$ involving a multistep rearrangement reaction is tested using the Master Equation formalism.

Introduction

In this paper we present a detailed study of the unimolecular dissociation of the methyl benzoate radical cation ($C_8H_8O_2^{+\bullet}$) aimed at understanding thermally driven dissociation reactions and how competition between different dissociation channels influence the product ion distributions. For example, direct bond cleavage reactions typically require high energy and precede through loose transition states, whereas rearrangement reactions require less energy and precede through tight transition states.[1,2] Various mass spectrometry techniques capable of sampling product ion distributions as a function of ion internal energy and/or lifetime of the dissociating ion have been used for studies of gas-phase unimolecular reactions. Such studies are important because differences in product ions or changes in relative abundance of the product ions with ion internal energy and/or ion lifetime can provide considerable insight into the nature of the unimolecular dissociation mechanisms. Furthermore, the experimental data obtained from such studies can be used to model the thermochemical behavior of the ions using a variety of electronic energy calculations and computational techniques. The $C_8H_8O_2^{+\bullet}$ radical cation is an excellent system for testing our understanding of unimolecular reactions because the ion dissociates to form multiple product ions (see Scheme 1) via competing reaction channels involving direct bond cleavage and rearrangement reactions, and this system has been extensively studied using a variety of experimental tools. Such a small molecule with limited degrees of freedom is also suited to relatively high level theoretical calculations, which can be used to refine the modeling of the dissociation process.

Audier et al.[3] used deuterium-labeled analogs ($C_6H_5COOCH_3$, $C_6H_5COOCD_3$, $C_6D_5COOCH_3$) and measured differences in the product ion abundances resulting from direct ionization and collision-induced dissociation (CID). They suggested that loss of $^{\bullet}OCH_3$ involves direct bond cleavage to form the benzoyl ion, whereas the other product ions are formed through rearrangement reactions. They also suggested that the dissociation reactions involving rearrangement occurs through an intermediate formed by 1,4 hydrogen atom migration from the methyl group to the carbonyl oxygen to form a distonic radical cation. Although similar intermediates have been suggested for other organic radical cations,[4−6] the authors did not proposed a specific mechanism for elimination of CO_2. Recently, Dechamps et al. proposed mechanisms for dissociation of metastable methyl benzoate ions;[7] however, the experimentally measured product ion branching ratios are not entirely consistent with their mechanisms. Specifically, the authors were unable to locate a transition state for the major unimolecular reaction channel, loss of CO_2, and this transition state is critical to the elucidation of the unimolecular reaction mechanism.

SCHEME 1

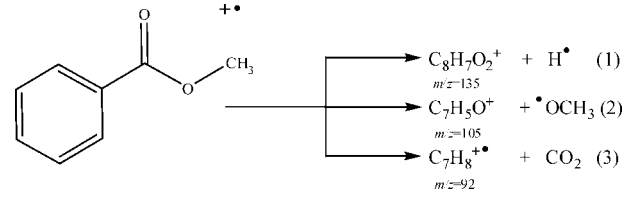

The present paper combines a wire ion-guide variant of blackbody infrared radiation dissociation (BIRD) using measurements of methyl benzoate radical cation decomposition kinetics with Master Equation simulations. The BIRD experiment is performed using a novel heated wire ion-guide ion trap (Fourier transform ion cyclotron resonance (FT-ICR) instrument),[8] and the Master Equation simulations were performed using a comprehensive multichannel mechanism developed using density function theory (DFT) calculations and using a collisional energy transfer model as an approximation to the radiative energy transfer kinetics. The dissociation reactions were studied using wire temperatures ranging from 670−1070 K. The goal of the study is to develop a detailed mechanism for the unimolecular reaction of methyl benzoate radical cation from first principles and to demonstrate the feasibility of the mechanism through kinetic modeling. In the Results and Discussion sections, the experimental results are provided first, followed by the discussion of a proposed dissociation mechanism and the associated DFT calculations. Finally, simulations

* To whom correspondence should be addressed. E-mail: russell@mail.chem.tamu.edu.

10.1021/jp7108048 CCC: $40.75
Published on Web 10/23/2008

of the experimental data based on the proposed mechanism using the Master Equation formalism are presented.

Experimental Methods

All experiments were carried out using a home-built FT-ICR mass spectrometer equipped with a two-section ion cell (dimensions of 7.62 cm × 3.18 cm × 3.18 cm), a 3.0 T Oxford superconducting magnet, and a Finnigan Odyssey data system. The ion cell vacuum is maintained by two Alcatel diffusion pumps, each backed with a mechanical pump. Ion gauges are located on each diffusion stack to measure the vacuum, and the vacuum gauge readings have been corrected for gauge sensitivity. The nominal base pressure for the vacuum system was less than 5×10^{-9} torr. A tungsten wire is positioned along the horizontal axis of the ICR cell, which can be resistively heated as a source of blackbody infrared radiation which induces dissociation of ions confined in the ion cell.[8] The heated wire ion-guide is positioned along the center line of the ion cell, and the tungsten electron emitter used to ionize the sample is positioned slightly off (3 mm) the horizontal axis of the cell. Therefore, ions generated by electron ionization are subjected to magnetron motion with an average radius that is approximately 3 mm away from the wire. This radius is small enough relative to the cell dimension so that the wire temperature can be used to approximate the temperature experienced by the ions inside cell. The temperature of the tungsten wire is controlled by varying the electrical current through the wire, and an infrared thermometer (Stamford, CT, Model 053707) is used to measure the tungsten wire temperature. A detailed procedure for the wire temperature control and measurement was described elsewhere.[8]

The temperature of the ion cell was calibrated by examining the temperature dependent unimolecular dissociation of the benzyl chloride radical cation ($C_7H_7Cl^{+\bullet}$).[8] In that study, the $C_7H_7^{+\bullet}$ is the only product ion that was detected, and a detailed kinetic analysis suggested that isomerization of benzyl chloride radical cation to chlorocycloheptatriene and chlorotoluene radical cations can occur at low (around 700 K) and high (higher than 930 K) wire temperatures, respectively. It is important to note that these studies serve to validate the wire ion-guide BIRD experiment and the results agree well with previous studies of the benzyl chloride ions,[9−12] and the derived energies for the isomeric $C_7H_7Cl^{+\bullet}$ ions (0.9 and 1.7 eV for benzyl chloride cation and chlorotoluene cations, respectively) are in very good agreement with data (1.1 and 1.6−1.8 eV for these two species, respectively) reported by Dunbar.[12]

Methyl benzoate was purchased from Sigma and used without further purification. The sample was introduced into the spectrometer using variable leak valves to achieve a static operating pressure of 1×10^{-8} to 2×10^{-7} torr. In all experiments the sample pressure was kept low in order to minimize ion−molecule reactions which yield protonated methyl benzoate ($C_8H_9O_2^+$, *m*/*z* 137). The sample was ionized at 15 eV electron ionization using a beam "on" time of 50 ms. The molecular ion was isolated after a 50 ms time delay by using stored waveform inverse Fourier transform (SWIFT). Following the SWIFT isolation event, the ions were allowed to react for time periods ranging from 250 ms to 20s and at the end of this period the relative abundances of the product ions were recorded.

The potential energy surfaces for dissociation of methyl benzoate radical cation were systemically explored using density functional theory (DFT) methods. All calculations were carried out using Gaussian G03 programs,[13] at the B3LYP/6-311++G(3d,2p) level of theory. The computational work was performed using the super computing facilities of Texas A&M University. The reactant and all product ions and intermediates were fully optimized and verified to be local minima based on frequency analysis. All transition states were verified to be the desired first order saddle points by both frequency analysis and intrinsic reaction coordinate (IRC) calculations. In all calculations, absolute zero enthalpies were estimated as electronic energies corrected by unscaled zero point vibrational energies.

The Master Equation methodology involves a set of coupled differential-integral equations that describe the chemical reaction and energy transfer rates for specified energy states.[14−17] For a single-channel, one-step unimolecular reaction containing only collisional excitation and deactivation, the time evolution of reacting population $g(E,t)$ with specific internal energy E can be expressed using the simplest form of Master Equation (eq 1)[16]

$$\partial g(E,t)\,\partial t = [\mathrm{M}]\int_0^\infty [R(E,E')g(E',t) - R(E',E)g(E,t)]dE' - k(E)g(E,t) \quad (1)$$

where [M] is the pressure of bath gas, $k(E)$ is the Rice−Ramsperger−Kassel−Marcus (RRKM) energy specific microscopic reaction rate coefficient, and $R(E,E')$ and $R(E',E)$ are the rate coefficients of the gain and loss of $g(E)$ by collisional energy transfer from and to all other energy levels of reactant molecules, respectively. Additional terms describing the absorption and emission of radiation can be added if necessary, although in the present work only collisional energy transfer terms were used in the modeling. The overall reaction rate constant can be expressed as the average rate coefficient over all available internal energy levels. For a complex system involving multichannel and multistep reactions, the Master Equations are coupled integral−differential equation sets containing all reaction channels and steps. The time evolution of the population fraction of methyl benzoate radical cations and all possible unimolecular dissociation products was obtained by numerically solving the Master Equations using the Multiwell program.[18−20] Specific details regarding procedures for setting up the Master Equations are discussed in the Results and Discussion section.

Results and Discussion

BIRD using both heated vacuum chambers and heated filaments has been extensively used by Williams to activate a range of gas-phase ions.[21] The present experiments differ from theirs in several important ways. Most notably is the fact that in Williams' experiments, the ions achieve equilibrium with the surroundings, thus the "temperature" of the dissociating ion is well defined, and in their heated filament experiment the heated filaments are located outside the ion cell and are far removed from the ion position. In our experiments the ions do not achieve equilibrium with the surrounding, i.e., the heated wire ion guide (WIG). On the other hand, in the heated WIG cell the effective temperature of the ions is much higher than can be obtained for equilibrium BIRD experiments. This is important because in the equilibrium BIRD experiments a limited number of fragmentation channels are observed, usually corresponding to the lowest energy reaction channels. The heated WIG cell has advantages of convenience, viz., the entire vacuum system does not have to be heated, and higher temperatures (> 1000 K) can be achieved. That is, high temperature dissociation channels not accessible through equilibrium BIRD experiments can be explored using the heated-WIG cell. Therefore, our experimental

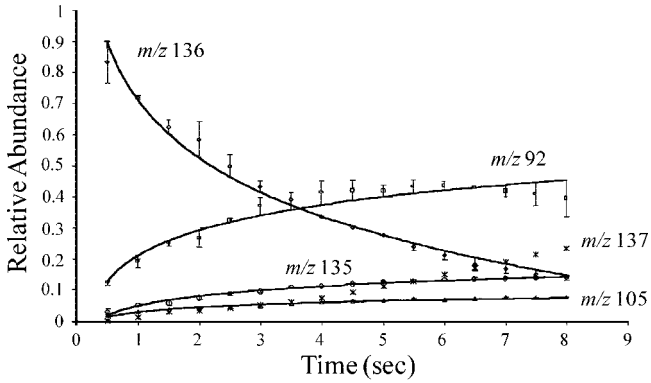

Figure 1. Temporal plot of the relative abundance of methyl benzoate cation and product ions at a WIG temperature of 890 K.

method can offer information complementary to that obtained via equilibrium BIRD, CID, and IRMPD.

The unimolecular dissociation of methyl benzoate radical cations ($C_8H_8O_2^{+\bullet}$) was examined by varying the WIG temperature and the pressure of neutral methyl benzoate in a FT-ICR cell.[8] A temporal plot of $C_8H_8O_2^{+\bullet}$ and the various product ion abundances formed by dissociation at 890 K are contained in Figure 1. An apparent $C_8H_8O_2^{+\bullet}$ ion dissociation rate constant (k_{exp}) was obtained from the slope of a plot of logarithm of relative ion abundance vs reaction time (see Figure 2). The temperature dependent k_{exp} values are listed in Table 1, and the relative abundances of each species at 890 and 1010 K measured at 1 s of reaction time are listed in Table 2. At the lower temperatures, the major product ion is formed by CO_2 loss (*m/z* 92) and ions formed by hydrogen atom ($H^\bullet$) (*m/z* 135) and $^\bullet OCH_3$ loss (*m/z* 105) are minor products. Note that at higher wire temperatures the relative abundance of the *m/z* 105 ion increases, whereas the $H^\bullet$ loss product ion (*m/z* 135) changes very little.

By use of the experimental results as a guide, we considered several possible reaction pathways by which $C_8H_8O_2^{+\bullet}$ radical cations dissociate to form *m/z* 92 (loss of CO_2), 105 (loss of $^\bullet OCH_3$), and 135 (loss of $H^\bullet$). DFT-based molecular orbital calculations were used to evaluate the energies of the reactants and transition states. In the following sections we describe a mechanism that is consistent with all the data, and in the final section of the paper we test our proposed mechanism using the Master Equation formalism.[14−20] In the discussion of the dissociation mechanism we use the term "energy barrier" of a transition state to mean the absolute zero enthalpy difference between the transition state and the initial energy of $C_8H_8O_2^{+\bullet}$ radical cation.

We first estimated the enthalpy change of methoxy radical loss from methyl benzoate radical cation by evaluating the electronic energy of $C_8H_8O_2^{+\bullet}$ as a function of carbonyl carbon methoxy oxygen bond distance, calculated at the B3LYP/6-311++G(3d,2p) level of theory. Because $^\bullet OCH_3$ loss is likely a simple bond cleavage reaction we allowed the C−O bond distance to vary in a stepwise manner and allowed all other geometric parameters to vary without restrictions. The calculations yield a C−O bond dissociation energy (BDE) of 30.9 kcal mol^{-1} (1.34 eV), which agrees very well with the value (1.35 eV) reported by Elder et al.[22] The energetics for loss of $^\bullet OCH_3$ provides an important reference point for developing a mechanism for CO_2 loss. For example, the temperature dependent data shows that loss of CO_2 is favored over $^\bullet OCH_3$ loss at lower temperatures, but methoxy radical loss begins to compete with rearrangement reaction channels at higher temperatures, thus the energy barrier for CO_2 loss must be lower than 1.34 eV, i.e., the BDE of direct $^\bullet OCH_3$.

At the B3LYP/6-311++G(3d,2p) level of theory, we also examined the energetics for the most straightforward mechanism for loss of CO_2, specifically 1,2-methyl migration from the ester group to the ortho position of phenyl ring followed by elimination of CO_2 (Figure 3). Note, however, that the energy barriers for this reaction pathway are much higher than BDE for $^\bullet OCH_3$ loss. For example, the energy barrier for methyl migration is ∼64 kcal mol^{-1}. We also considered intramolecular hydrogen transfer from the methyl group to the carbonyl oxygen (Figure 4) to form the distonic ion **5**, followed by a series of rearrangement reactions to form **8,** which then undergoes ipso-hydrogen migration followed by elimination of CO_2, but the energetics for these processes exceed the limit imposed by the BDE for $^\bullet OCH_3$ loss and we concluded that this is an unlikely mechanism.

The mechanism depicted in Figure 5 yields the best agreement between experimental data and molecular orbital calculations for the CO_2 loss, i.e., rearrangement of the $C_8H_8O_2^{+\bullet}$ ion to form a hemiketal bicyclic ion (structure 11) (Figure 5), which undergoes a series of hydrogen transfer reactions and ring-opening of the 5-membered ring and CO_2 elimination involving electrophilic hydrogen transfer from the −COOH group to the ortho and para positions of 6-membered ring and methylene carbon atom. The final products of these reactions comprise a mixture of toluene, *p*-isololuene, and *o*-isotoluene radical cations. The overall exothermicities of these reactions are of −29, −19, and −22 kcal mol^{-1}, respectively, and it appears that the rate-determining step for this pathway is the 5,6-hydrogen migration (see Scheme 2), which has an energy barrier of 27 kcal mol^{-1}, about 4 kcal mol^{-1} lower in energy than the direct bond cleavage pathway for $^\bullet OCH_3$ loss. However, if the reacting system follows a "hydrogen scrambling" pathway, we would expect to observe predominant $H^\bullet$ loss instead of CO_2 loss because the energy barrier for hydrogen atom loss from position 1 of structure 11 (see Scheme 2) is about 24 kcal mol^{-1} lower than that of the rate-determining step of CO_2 loss by 3.0 kcal mol^{-1}. Obviously, this pathway still needs to be investigated further and the relevant discussion will be given below.

The mechanism contained in Figure 5 is similar to one proposed by Dechamps et al.[7] differing only in the intramolecular proton transfer (structure 17) from the COOH group to the 6-membered ring and simultaneous elimination of CO_2, resulting in the formation of a mixture of $C_7H_8^{+\bullet}$ radical cations, structures 18, 19, and 20). Dechamps proposed a direct cleavage of HCO_2 from complex 17, forming HCO_2−toluene (or *o*-isotoluene) complex, followed by the loss of neutral CO_2 via intracomplex proton transfer, forming a mixture of toluene and *o*-isotoluene radical cation.[7,23]

A second mechanism proposed by Dechamps involved a 5-membered ring-opening reaction occurring before hydrogen migration along the 6-membered ring, or 5-membered ring opening occurs at the structure illustrated in Scheme 2).[7] This mechanism is more probable compared to the "hydrogen-scrambling" pathway, because 5-membered ring opening prior to the hydrogen scrambling along the 6-membered ring lowers the energy barrier for the rate-determining step. The Dechamps CO_2 loss mechanism has a slightly lower energy barrier (22.2 kcal mol^{-1}) than that for hydrogen atom loss from C-1 of 11 (22.7 kcal mol^{-1}); however, the energy difference between CO_2 loss and hydrogen atom loss is only 0.5 kcal mol^{-1}, and the current single-reference based density functional theory calculations cannot achieve such a high "chemical accuracy". There-

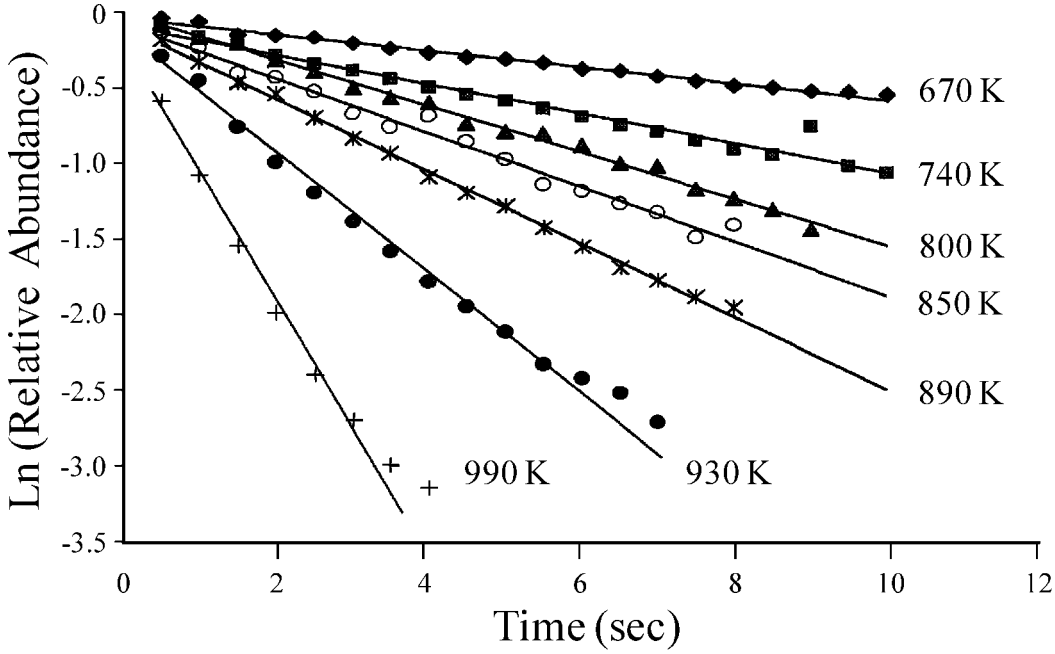

Figure 2. Plots of the logarithm of the relative abundance for methyl benzoate radical cation vs reaction time at different temperatures.

TABLE 1: Experimentally Measured and Theoretically Estimated Apparent Depletion Rate Constants (s^{-1}) of the $C_8H_8O_2^{+\bullet}$ ion as Well as the Parameter C_1 Used in Master Equation Calculations

temperature (K)	k_{exp}[a]	k_{sim}[b]	C_1 (cm^{-1})
670	0.053	0.053	390
740	0.096	0.12	500
850	0.18	0.21	550
890	0.24	0.29	620
990	0.75	0.76	960
1020	1.2	1.3	1800
1035	1.4	1.3	2300
1070	1.9	1.5	3620

[a] FT-ICR experimental results; see ref 8. [b] Master Equation simulation results.

TABLE 2: Relative Abundance of Reactants and Products

	890 K		1010 K	
	experimental values[a]	theoretical prediction	experimental values[a]	theoretical prediction
reactant	0.71	0.72	0.24	0.30
CO_2 loss	0.19	0.27	0.46	0.56
$^{\bullet}OCH_3$ loss	0.034	0.00020	0.18	0.11
$H^{\bullet}$ loss	0.059	0.0082	0.13	0.026

[a] Experimental values are obtained by measuring the relevant ion peak intensities of the spectra shown in ref 8.

fore, neither mechanism proposed by Dechamps provides a very convincing rationale for favoring CO_2 loss over hydrogen atom loss.

We calculated the energetics for three reaction channels (Scheme 2 is the starting point for the calculations), and the results are summarized in Table 3. It appears that hydrogen atom loss is associated with an energy barrier of at least 19.3 kcal mol^{-1}. For example, if hydrogen atom loss occurs at position 3 with energy barrier of 19.3 kcal mol then the system (starting from structure 11) must undergo two consecutive hydrogen migrations from positions 1 and 3, with the energy barriers of 18.6 and 19.3 kcal mol^{-1}, respectively. On the other hand, ring opening can occur at these two positions, especially at position 2 (with energy barrier of only 9.7 kcal mol^{-1}); thus it is more likely that the ring opening occurs before the hydrogen atom loss. As long as ring opening has already occurred, it becomes more difficult to lose a hydrogen atom owing to the high reaction endothermicity (39.8 kcal mol^{-1}). The same conclusion can be drawn for the $H^{\bullet}$ loss at other positions. Thus, it appears that CO_2 loss is favored over $H^{\bullet}$ loss.

On the basis of the above discussion we derived the following mechanism for the unimolecular dissociation of methyl benzoate radical cation: the initially formed radical cation rearranges to an α-distonic structure 5 and bicyclic structure 11. Starting from intermediate 11, it is most likely that the hydrogen migration to position 6 with 5-membered ring opening occurring prior to hydrogen migration and CO_2 loss can be achieved before hydrogen atom loss can from the sp^3 carbon of 6-membered ring owing to the energy difference between $H^{\bullet}$ loss and the rate-determining step of CO_2 loss.

The proposed mechanism was analyzed by using a Master Equation approach to model two extremes: the rapid-exchange and slow-exchange limits.[14−20] In the rapid-exchange limit, the application of canonical transition state theory (CTST) is appropriate for the treatment of unimolecular reactions.[24] The initial energy distribution of methyl benzoate ions is assumed to be adequately described by a Boltzmann distribution at the wire temperature independent of the internal energy distribution arising from electron impact ionization. In the case of BIRD experiments this limit is realized when the rates of radiative absorption and emission are rapid compared to unimolecular reaction rates, i.e., for high photon density and/or large ions. Although such criteria may not be valid for our experiments, we performed CTST simulations using Multiwell software based on the proposed mechanism. We assumed an artificial pressure of one atmosphere (760 torr) to simulate the rapid-exchange limit. The canonical rate constant (k_c) for each reaction step is expressed as

$$k_c = (k_B/h)\exp(-\Delta G/RT) \quad (2)$$

where T is absolute temperature, R is ideal gas constant, k_B is Boltzmann constant, h is Planck's constant, and ΔG is the Gibbs free energy difference between the transition state and the

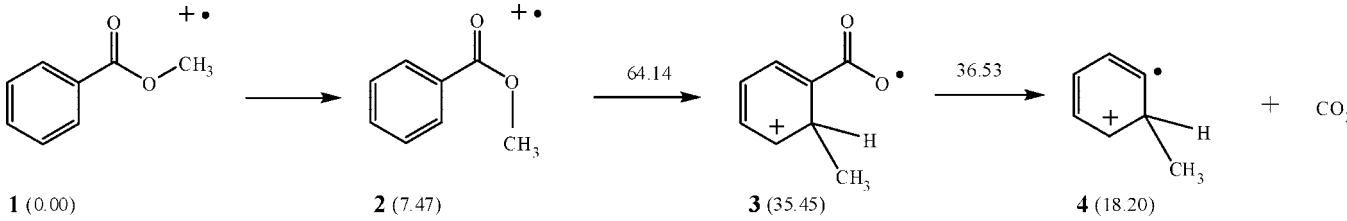

Figure 3. The reaction sequence for the dissociation of methyl benzoate radical cation involving methyl migration. The numbers in brackets are the energies of local minima and the numbers above the arrows are the energies of transition states. All values are given in kcal mol^{-1}.

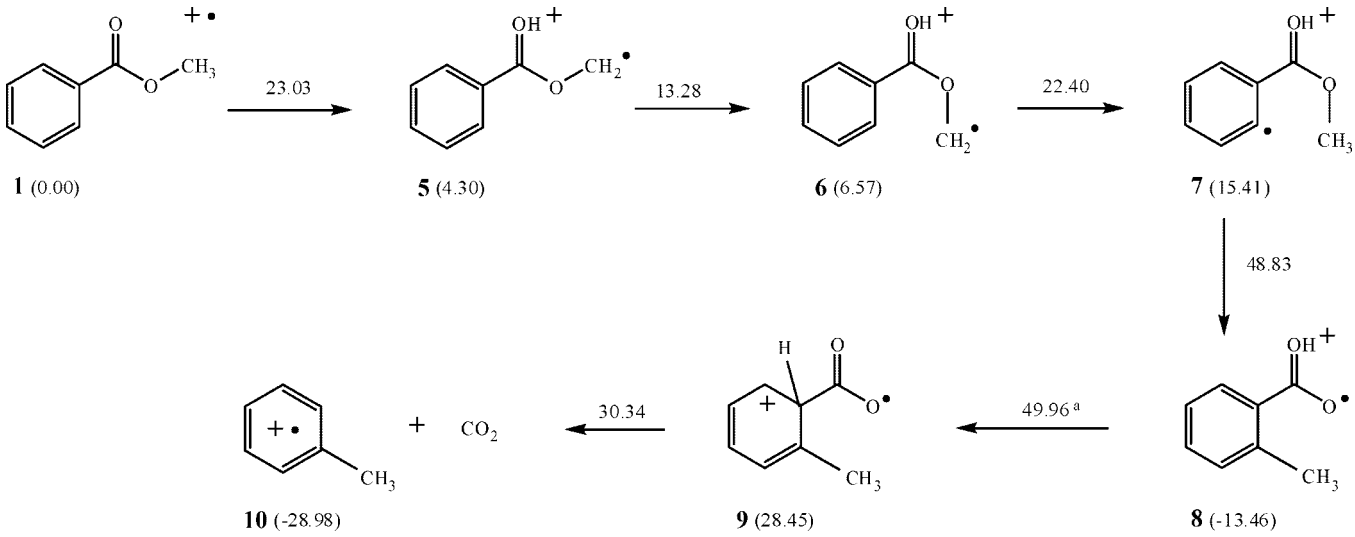

Figure 4. The reaction sequence for the dissociation of methyl benzoate radical cation involving ipso hydrogen migration. The numbers in brackets are the energies of local minima and the numbers above the arrows are the energies of transition states. All numbers are given in kcal mol^{-1}.

reactant ion. The results of the CTST calculations are shown in Figure 6. Clearly, the results from simulation of the data from 890 K are inconsistent with the experimental data. The decomposition rates of the parent ions and the temperature-dependent branching ratios of the product ions do not match the experimental data. These results are not surprising considering that Dunbar previously showed that the energy distributions of small molecule ions with less than 300 degrees of freedom are truncated.[25]

The slow-exchange limit is realized when the collisional energy transfer is significantly slower than the dissociation rate, i.e., the time-dependent behavior is a strong function of the initial internal energy distribution of the ions, specifically those ions with energy above the dissociation threshold. Under these conditions ions with energies below the dissociation threshold are stable and additional energy must be provided for dissociation to occur. In more conventional BIRD experiments, this limit is achieved when the photon density is low and the unimolecular reaction rates are significantly larger than the radiative absorption and emission rates. These conditions were modeled by assuming microcanonical internal energy distribution. The lower panel of Figure 6 shows the results from RRKM calculation are also consistent with microcanonical initial internal energy distribution of 32 kcal mol^{-1} relative to the absolute zero enthalpy of reactant ion, i.e., 1 kcal mol^{-1} above the threshold for direct bond cleavage. The results from RRKM calculations are inconsistent with experimental observations. In addition, since there is no energy transfer in this limit there should be no temperature dependence to either the decomposition rates or the product-branching ratios, which is also inconsistent with experiment.

The implications for modeling of both the rapid and slow-exchange limits is that the kinetic treatment must include explicit energy transfer in order to reproduce experimental results; thus the Master equation is an adequate tool for modeling this system. The Multiwell code Master Equation calculations include all energy specific RRKM microcanonical rate constants $k(E)$ and density of states, estimated from DFT calculated vibrational frequencies and rotational constants, of all species involved. The only exception is the $^{\bullet}OCH_3$ direct cleavage channel, which is associated with a loose transition state and the $k(E)$ value for this process was determined using inverse transform method,[25] with pre-exponential factor A^{∞} assumed to be 10^{16}, a typical value for direct bond cleavage via a loose transition state.[16,26] To apply the Master Equation formalism we need to address two issues: (1) the nature of initial energy distribution and (2) the inclusion of energy-transfer processes.

In both rapid- and slow-exchange limiting cases the calculated reaction rates are much faster than the experimental values, which implies that ions with excess internal energy will not survive the time delay (~50 ms) between ion formation and isolation by SWIFT; therefore, a truncated Boltzmann distribution (the high energy part of the ions is eliminated from the overall ion population) is an appropriate initial energy distribution. The truncation (represented in terms of the highest vibrational energy state occupied by the methyl benzoate cation) was applied at 8075 cm^{-1}, slightly above the threshold of the rate-determining step of CO_2 loss channel (8060 cm^{-1}).

It is also important to note that the simulation of BIRD data in the intermediate regime, i.e., radiative absorption and emission compete with unimolecular dissociation, has been previously discussed by Dunbar.[27] Approximations to the modeling (such as weakly coupled harmonic oscillator and linear scaling of infrared intensities with total number of internal degrees of freedom) have been successfully applied to a number of model hydrocarbon ions; however, the methyl benzoate system rep-

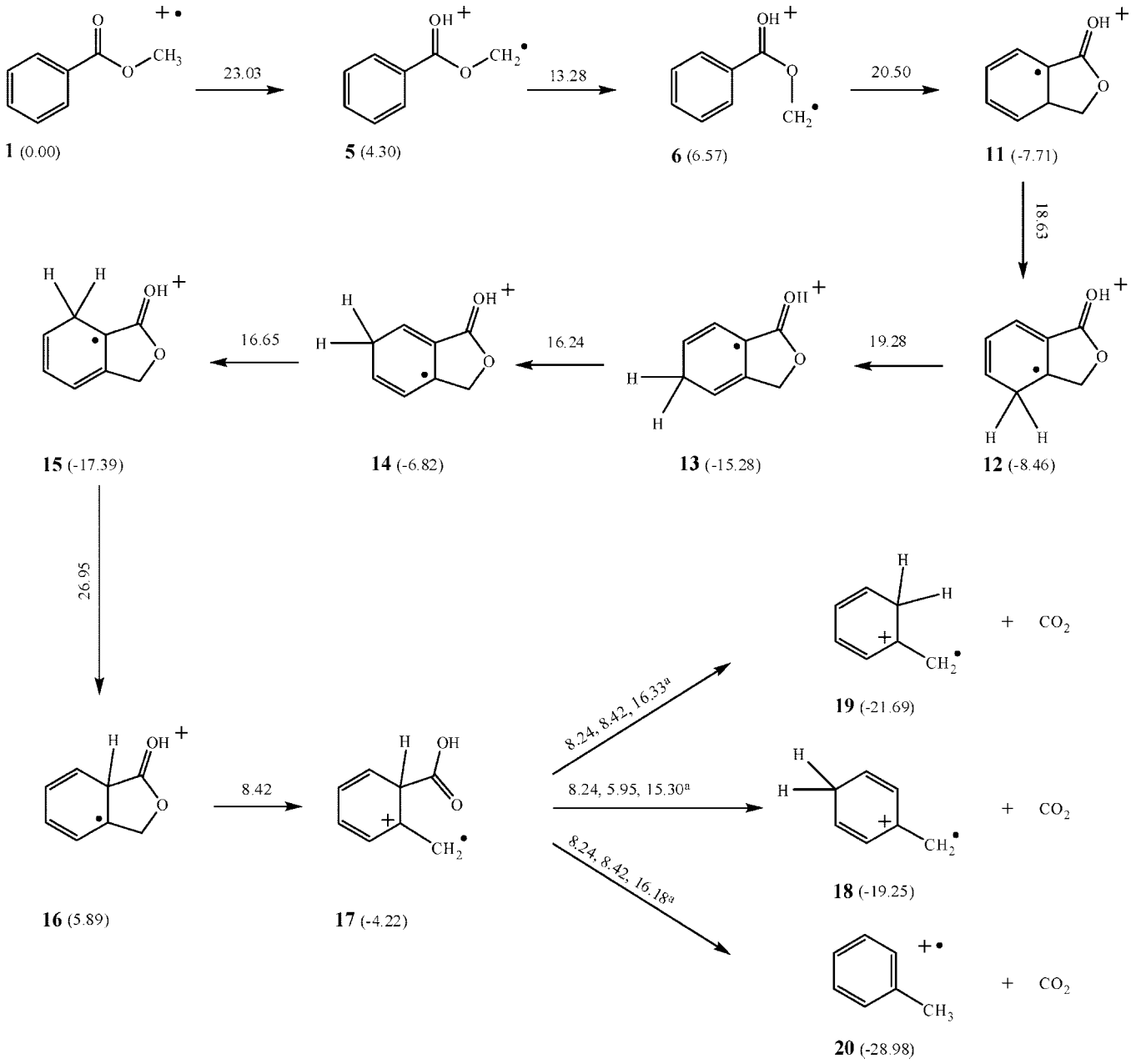

Figure 5. The reaction sequence for the dissociation of methyl benzoate radical cation involving indirect 1,6 hydrogen migration. The numbers in brackets are the energies of local minima, and the numbers above the arrows are the energies of transition states. All numbers are given in kcal mol^{-1}. The first two numbers are the energy barriers for the two consecutive rotation of COOH group.

SCHEME 2

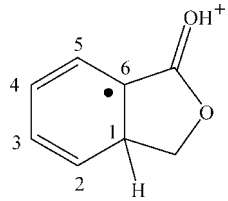

resents a particularly challenging example for several reasons: (i) the system involves three reaction pathways (CO_2, H• and •OCH_3 loss), 18 wells (intermediates), and 31 total possible reaction channels, so that accurate modeling of the absorption and emission processes for all the intermediates is prohibitive; (ii) the current version of Multiwell program does not take into account the energy-transfer channels for radiative absorption and emission. Our goal is to model the energy-transfer process semiquantitatively so that both the experimental dissociation kinetics and product branching ratios can be reproduced. Although we cannot directly model photon radiation, we can

TABLE 3: Energy Barriers (kcal mol^{-1}) for Hydrogen Migration along the 6-Membered Ring, Hydrogen Atom Loss, and 5-Membered Ring Opening for Each sp^3 C Position[a]

sp^3 carbon position	H atom migration	H atom loss	ring-opening	H atom migration after ring opening	H atom loss after ring opening
1	18.6 (19.4)	22.3 (22.7)	21.9 (21.8)	22.5 (22.2)	not found
2	19.3 (21.0)	21.0	9.7	14.0 (13.6)	40.9
3	16.2 (16.7)	19.3	14.0	16.8 (16.0)	not found
4	16.7 (17.2)	21.4	6.8	14.5 (14.2)	40.3
5	27.0 (27.5)	19.5	14.3	16.4 (16.0)	not found
6	N/A	not found	8.4	N/A	42.1

[a] The numbers in brackets are converted from the data given in ref 7. The numbering of carbon positions is illustrated in scheme 2.

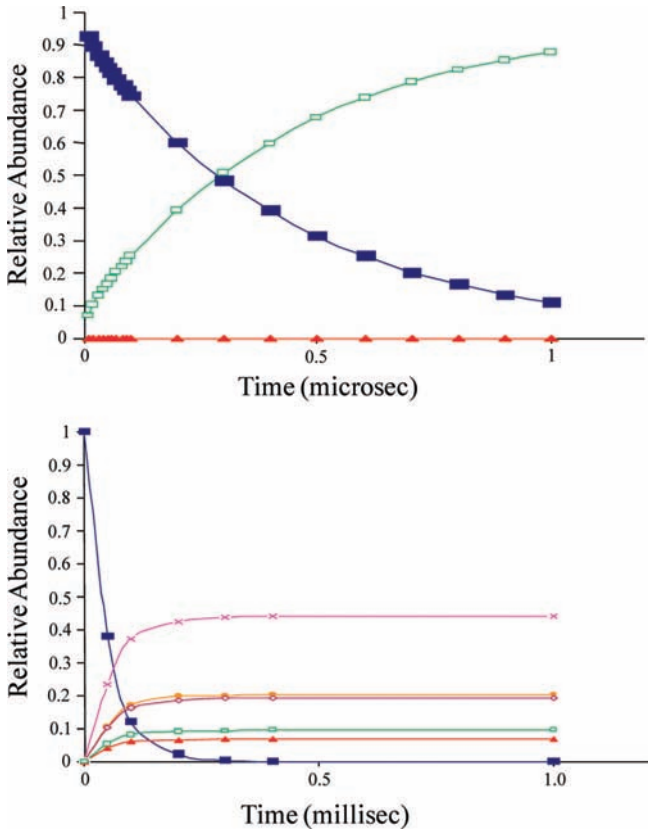

Figure 6. Upper panel: The time evolution of methyl benzoate and product ions at 890 K, calculated using canonical transition state theory. The pressure is assumed to be 1 atm for the rapid-exchange limit. In the figure, except for reactant and methoxy loss product ions, the abundances of all other product ions are very low and the curves for these ions overlap. Lower panel: The time evolution of methyl benzoate and product ions at 890 K, calculated using RRKM theorem, using an internal energy value of 32 kcal mol^{-1} (1 kcal mol^{-1} above the threshold value of $^{\bullet}OCH_3$ cleavage channel): ■, $C_8H_8O_2^{+\bullet}$; □; $-{}^{\bullet}OCH_3$, ▲, $-H^{\bullet}$, ×, *p*-isotoluene cation, ●, *o*-isotoluene cation; ○, toluene cation.

estimate the importance of such processes by approximating radiation-induced energy transfer using a collisional energy transfer model. For example, here we use collisional energy transfer model within the Multiwell code to include the role of energy transfer. A single exponential model was used for the energy transfer rate calculation based on eq 3[16]

$$P_{down}=\exp(-(E_1-E_2)/C_1) \quad (3)$$

where P_{down} is the probability of energy transfer event in which a species with internal energy E_1 will change its energy to E_2 upon collision ($E_1 > E_2$). C_1 is an adjustable parameter, which is equal to $\langle\Delta E\rangle_{down}$, the average energy loss per collision. The actual parameters used for modeling the energy transfer process are not critical. The neutral methyl benzoate was assumed to be the neutral bath gas, with Lennard-Jones parameters σ = 6.63 Å and ϵ/k_B = 425.29 (K), calculated by the method suggested by Mourits and Rummens, using the critical temperature (692 K) and pressure (2.3×10^{-7} torr) of methyl benzoate. In this model the probability of energy gain is related to the energy loss probability through detailed balance.

The Master Equation derived temporal plots for $C_8H_8O_2^{+\bullet}$ ions and the product ions *m*/*z* 135, 105, and 92 at 890 and 1070 K are contained in Figures 7 and 8, respectively. The overall apparent reaction rates at different temperatures were derived from the slope of natural logarithm plots of simulated ion abundance for $C_8H_8O_2^{+\bullet}$ ions vs time, and these values as well

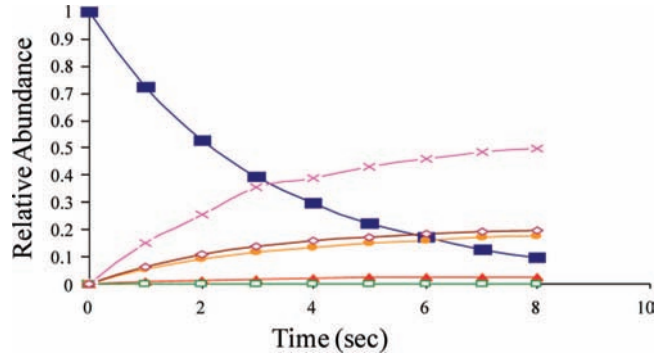

Figure 7. Temporal plots of relative abundance of methyl benzoate radical cation (*m*/*z* 136) and the dissociation product ions obtained from the Master Equation simulations at a temperature of 890 K. ■, $C_8H_8O_2^{+\bullet}$; □, $-{}^{\bullet}OCH_3$; ▲, $-H^{\bullet}$; ×, *p*-isotoluene cation; ●, *o*-isotoluene cation; ○, toluene cation.

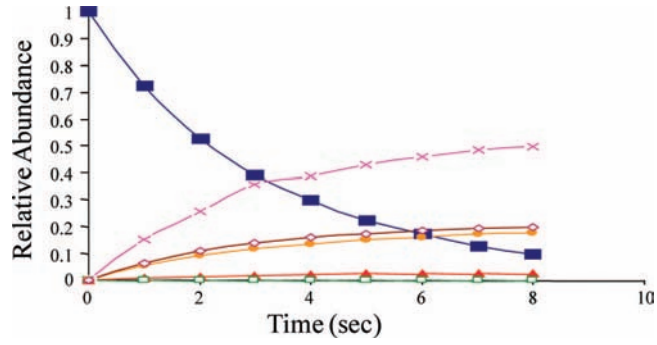

Figure 8. Temporal plots of relative abundance of methyl benzoate radical cation (*m*/*z* 136) and the dissociation product ions obtained from the Master Equation simulations at a temperature of 1070 K. ■, $C_8H_8O_2^{+\bullet}$; □, $-{}^{\bullet}OCH_3$; ▲, $-H^{\bullet}$; ×, *p*-isotoluene cation; ●, *o*-isotoluene cation; ○, toluene cation.

as the experimental data are listed in Table 1. The experimentally measured and the Master Equation simulated relative abundances of all reacting species at 890 and 1010 K are listed in Table 2.

Clearly the Master Equation simulations reproduce the experimental data and thus validate our proposed dissociation mechanism. It is important to note that the goal of these simulations *is not to extract accurate thresholds* but rather to provide a connection between a proposed mechanism and the experimental data with minimal adjustable parameters. The treatment is relatively easy to implement for complex multichannel dissociation and microscopic reversibility. The choice of neutral bath gas pressure of 2.3×10^{-7} torr and C_1 of 620 cm^{-1} used to fit the dissociation rate at 890 K is arbitrary since both parameters determine the energy transfer rates, the first in determining the collision frequency and the second in determining the efficiency of energy transfer. For the remaining temperatures the value of C_1 was adjusted to fit the parent dissociation rates. It is important to note that two parameters, experimental error and energy grain size, of the Master Equation most strongly affect the quality of the fits. As noted above, our goal is to provide reasonable agreement between experimental and modeled ion abundances. As seen from the data contained in Table 1, the C_1 values increase with temperature as is expected. Although a weak temperature dependence for C_1 in collisional models is typical,[16] the strong temperature dependence for C_1 has a physical basis in the strong dependence of the wire emission as a function of temperature. What is significant about the results of this modeling is not that the agreement with the experimental unimolecular dissociation rates

can be achieved, in fact it is unremarkable given the parametrization, but that the relative branching of reacting channels are reproduced (including their temperature-dependence). Since the modeling fixes the threshold energies and vibrational frequencies to the DFT values, in effect fixing the microcanonical rates, the agreement of the branching ratios with experiments strongly suggests that the proposed mechanism is correct.

Conclusions

In this research, we studied blackbody infrared radiation induced unimolecular dissociation of methyl benzoate radical cation generated via electron ionization in FT-ICR mass spectrometers. We found that, at low temperature, the major fragmentation pathway of $C_8H_8O_2^{+\bullet}$ is CO_2 loss although the hydrogen atom loss and $^{\bullet}OCH_3$ loss are also detected. When the FT-ICR cell temperature increases, $^{\bullet}OCH_3$ loss begins to compete with the other fragmentation channels.

We suggested reaction mechanisms of methyl benzoate cation dissociation based upon those experimental results. According to our most probable mechanism, the $^{\bullet}OCH_3$ loss is best described as direct bond cleavage, while the CO_2 loss and hydrogen atom loss occur via a series of rearrangements. A hemiketal bicyclic intermediate involves formation of a distonic enol-type methyl benzoate cation. This bicyclic intermediate can undergo further reactions through competitive channels of the five-membered ring opening, hydrogen atom loss, and hydrogen migration along the six-membered ring. The preference for CO_2 loss and $^{\bullet}OCH_3$ loss can be predicted by this mechanism, in agreement with the product branching ratios observed from FT-ICR experiments. Master Equation calculations support the proposed mechanism.

Acknowledgment. This work was supported by the Robert A. Welch Foundation (A-1176-DHR, A-1405-SWN) and the U.S. Department of Energy, Division of Chemical Sciences/BES. Y. Huang also thanks Dr. John Barker and Dr. Andrea Maranzana (University of Michigan) for their guidance in the utilization of Multiwell program and Dr. R. C. Dunbar (Case Western Reserve University) for his insightful comments. The assistance offered by Dr. Lisa M. Perez (Laboratory for Molecular Simulation, Texas A&M University) is also greatly appreciated.

References and Notes

(1) Baer, T.; Dutuit, O.; Mestdagh, H.; Rolando, C. *J. Phys. Chem.* **1988**, *92*, 5674–5679.

(2) Muntean, F.; Armentrout, P. B. *J. Phys. Chem. A* **2003**, *107*, 7413–7422.

(3) Audier, H. E.; Milliet, A.; Sozzi, G.; Hammerum, S. *Org. Mass Spectrom.* **1990**, *25*, 44–48.

(4) Heinrich, N.; Schmidt, J.; Schwarz, H.; Apeloig, Y. *J. Am. Chem. Soc.* **1987**, *109*, 1317–1322.

(5) Audier, H. E.; Milliet, A. *Org. Mass Spectrom.* **1980**, *15*, 477–482.

(6) Grutzmacher, H. F. *Int. J. Mass Spectrom. Ion Process.* **1992**, *118/119*, 825–855.

(7) Dechamps, N.; Flammang, R.; Gerbaux, P.; Nam, P.; Nguyen, M. T. *J. Am. Soc. Mass Spectrom.* **2006**, *17*, 807–814.

(8) Peterman, S. *Development and Implementation of an in Situ Blackbody Infrared Radiation Source in a FT-ICR Mass Spectrometer, in Chemistry*; Texas A&M University: College Station, 2001.

(9) Jo Jackson, J-A. A.; Lias, S. G.; Ausloos, P. *J. Am. Chem. Soc.* **1977**, *99*, 7515–7521.

(10) Honovich, J. P.; Dunbar, R. C. *Int. J. Mass. Spectrom. Ion Process.* **1982**, *42*, 33–42.

(11) Proctor, C. J.; McLafferty, F. W. *Org. Mass. Spectrom.* **1983**, *18*, 193–197.

(12) Fu, E. W.; Dymerski, P. P.; Dunbar, R. C. *J. Am. Chem. Soc.* **1976**, *98*, 337–342.

(13) Frisch, M. J.; Trucks, G. W.; Schlegel, H. B.; Scuseria, G. E.; Robb, M. A.; Cheeseman, J. R.; Zakrzewski, V. G.; Montgomery, J. A., Jr.; Stratmann, R. E.; Burant, J. C.; Dapprich, S.; Millam, J. M.; Daniels, A. D.; Kudin, K. N.; Strain, M. C.; Farkas, O.; Tomasi, J.; Barone, V.; Cossi, M.; Cammi, R.; Mennucci, B.; Pomelli, C.; Adamo, C.; Clifford, S.; Ochterski, J.; Petersson, G. A.; Ayala, P. Y.; Cui, Q.; Morokuma, K.; Salvador, P.; Dannenberg, J. J.; Malick, D. K.; Rabuck, A. D.; Raghavachari, K.; Foresman, J. B.; Cioslowski, J.; Ortiz, J. V.; Baboul, A. G.; Stefanov, B. B.; Liu, G.; Liashenko, A.; Piskorz, P.; Komaromi, I.; Gomperts, R.; Martin, R. L.; Fox, D. J.; Keith, T.; Al-Laham, M. A.; Peng, C. Y.; Nanayakkara, A.; Challacombe, M.; Gill, P. M.W.; Johnson, B.; Chen, W.; Wong, M. W.; Andres, J. L.; Gonzalez, C.; Head-Gordon, M.; Replogle, E. S.; Pople, J. A. *Gaussian 03*; Gaussian, Inc.; Pittsburgh, PA, 2001.

(14) Miller, J. A.; Klippenstein, S. J. *J. Phys. Chem. A* **2006**, *110*, 10528–10544.

(15) Bedanov, V. M.; Tsang, W.; Zachariah, M. R. *J. Phys. Chem.* **1995**, *99*, 11452–11457.

(16) Gilbert, R. G.; Smith, S. C. *Theory of Unimolecular and Recombination Reactions*; Oxford:Blackwell, 1990.

(17) Steinfeld, J. I.; Francisco, J. S.; Hase, W. L. *Chemical Kinetics and Dynamics*, 2nd ed.; Prentice Hall: New Jersey, 1999.

(18) Barker, J. R. *Multiwell 2.0*; University of Michigan: Ann Arbor, MI, 2006.

(19) Barker, J. R. *Int. J. Chem. Kinetics* **2001**, *33*, 232–245.

(20) Barker, J. R.; Ortiz, N. F. *Int. J. Chem. Kinetics* **2001**, *33*, 246–261.

(21) Wong, R. L.; Robinson, E. W.; Williams, E. R. *Int. J. Mass. Spectrom.* **2004**, *234*, 1–9.

(22) Elder, J. F.; Beynon, J. H.; Cooks, R. G. *Org. Mass. Spectrom.* **1976**, *11*, 415–422.

(23) Dechamps, N.; Flammang, R.; Gerbaux, P.; Nam, P.; Nguyen, M. T. *Chem. Phys. Lett.* **2006**, *419*, 139–143.

(24) Robinson, P. J.; Holbrook, K. A. *Unimolecular Reactions*; Wiley-Interscience: London, NY, 1972.

(25) Baer, T.; Hase, W. L. *Unimolecular reaction dynamics: theory and experiments*; Oxford University Press: New York, 1996.

(26) Price, W. D.; Schnier, P. D.; Jockusch, R. A.; Strittmatter, E. F.; Williams, E. R. *J. Am. Chem. Soc.* **1996**, *118*, 10640–10644.

(27) Dunbar, R. C. *J. Phys. Chem.* **1994**, *98*, 8705–8712.

(28) Mourits, F. M.; Rummens, F. H. A. *Can. J. Chem.* **1977**, *55*, 3007–3020.

JP7108048